# High-Resolution Frequency-Wavenumber Spectrum Analysis

J. CAPON, MEMBER, IEEE

**Abstract**—The output of an array of sensors is considered to be a homogeneous random field. In this case there is a spectral representation for this field, similar to that for stationary random processes, which consists of a superposition of traveling waves. The frequency-wavenumber power spectral density provides the mean-square value for the amplitudes of these waves and is of considerable importance in the analysis of propagating waves by means of an array of sensors.

The conventional method of frequency-wavenumber power spectral density estimation uses a fixed wavenumber window and its resolution is determined essentially by the beam pattern of the array of sensors. A high-resolution method of estimation is introduced which employs a wavenumber window whose shape changes and is a function of the wavenumber at which an estimate is obtained. It is shown that the wavenumber resolution of this method is considerably better than that of the conventional method.

Application of these results is given to seismic data obtained from the large aperture seismic array located in eastern Montana. In addition, the application of the high-resolution method to other areas, such as radar, sonar, and radio astronomy, is indicated.

## Introduction

THE USE of an array of sensors for determining the properties of propagating waves is of considerable importance in many areas. As an example, such phased arrays find application in radar, where an array of receiving antennas is used to determine the spatial coordinates of radar targets. In seismic applications, the large aperture seismic array (LASA) [1] located in eastern Montana, is used to determine the vector velocity of propagating seismic waves. In addition, LASA provides seismic data for facilitating the discrimination between earthquakes and underground nuclear explosions.

The present work will be concerned with the use of an array of sensors to determine the vector velocity of propagating waves. In particular, the heavy emphasis will be on the seismic application based on seismic data obtained from LASA.

It is well known that a stationary random process can be characterized by means of a spectral density function [2]. Roughly speaking, this function provides the information concerning the power as a function of frequency for the stationary random process. In a similar manner, propagating waves, or a homogeneous random field, can be characterized by a frequency-wavenumber spectral density function. Loosely speaking, this function provides the information concerning the power as a function of frequency and the vector velocities of the propagating waves. The definition and properties of the frequency-wavenumber spectrum will be given subsequently. However, the main purpose of the present work is to discuss the measurement, or estimation, of the frequency-wavenumber spectrum. Previous methods of estimation were based on the use, at a given frequency, of a fixed wavenumber window. These conventional methods were limited to a wavenumber resolution which was determined primarily by the natural beam pattern of the array, as will be shown subsequently.

A high-resolution estimation method will be introduced which is based on the use of a wavenumber window which is not fixed, but is variable at each wavenumber considered. As a consequence, it will be shown that the wavenumber resolution achievable by this method is considerably greater than that of the conventional method and is limited primarily by signal-to-noise ratio considerations. The high-resolution method will be illustrated by examples obtained using LASA data consisting of long-period noise, long-period Rayleigh surface wave events, and short-period noise. Applications of the high-resolution method to other areas, such as radio astronomy, will also be indicated.

## Definition and Properties of the Frequency-Wavenumber Spectrum

We assume that the output of a sensor located at the vector position $\boldsymbol{x}_j$ is a wide-sense stationary discrete-time parameter random process with zero mean, $\{N_{jm}\}$, $m=0, \pm 1, \pm 2, \cdots$. The covariance matrix of the noise is given by

$$\rho_{jl}(m-n) = E\{N_{jm}N_{ln}^*\}, \tag{1}$$

where $E$ denotes expectation. The cross-power spectral density is

$$f_{jl}(\lambda) = \sum_{m=-\infty}^{\infty} \rho_{jl}(m)\varepsilon^{im\lambda}, \tag{2}$$

and

$$\rho_{jl}(m) = \int_{-\pi}^{\pi} f_{jl}(\lambda)\varepsilon^{-im\lambda}\frac{d\lambda}{2\pi}, \tag{3}$$

where $\lambda = 2\pi f T$ is the normalized frequency, $f$ is the frequency in hertz and $T$ is the sampling period of the data in seconds.

If the sensor output field is space stationary, then for fixed $\lambda$, $f_{jl}(\lambda)$ depends only on the vector difference $\boldsymbol{x}_j - \boldsymbol{x}_l$. In this case the sensor outputs are said to comprise a homogeneous random field, cf. Yaglom [2, pp. 81–84], and it is convenient to introduce a cross-power spectral density

Manuscript received December 13, 1968; revised June 17, 1969.

The author is with M.I.T. Lincoln Laboratory, Lexington, Mass. (Operated with support from the U. S. Advanced Research Projects Agency.)

$f(\lambda, \boldsymbol{r})$ and cross-covariance $\rho(m, \boldsymbol{r})$ as

$$f(\lambda, \boldsymbol{r}) = f_{jl}(\lambda), \tag{4}$$

$$\rho(m, \boldsymbol{r}) = \rho_{jl}(m), \tag{5}$$

whenever $\boldsymbol{x}_j - \boldsymbol{x}_l = \boldsymbol{r}$.

Following Yaglom, [2, pp. 81–84], any homogeneous random field has a spectral representation

$$N_{jm} = \int_{-\pi}^{\pi}\int_{-\infty}^{\infty}\int_{-\infty}^{\infty} \varepsilon^{-i(m\lambda + \boldsymbol{k}\cdot\boldsymbol{x}_j)} Z(d\lambda, d\boldsymbol{k}) \tag{6}$$

where $\boldsymbol{k}$ is the vector wavenumber. We have that $Z(\Delta\lambda, \Delta\boldsymbol{k})$ is a random function of the frequency interval $\Delta\lambda$ and the elemental wavenumber area, or interval $\Delta\boldsymbol{k}$, with the following properties:

1) $E\{Z(\Delta\lambda, \Delta\boldsymbol{k})\} = 0$, for all $\Delta\lambda, \Delta\boldsymbol{k}$;
2) $Z(\Delta\lambda, \Delta_1\boldsymbol{k} + \Delta_2\boldsymbol{k}) = Z(\Delta\lambda, \Delta_1\boldsymbol{k}) + Z(\Delta\lambda, \Delta_2\boldsymbol{k})$, if $\Delta_1\boldsymbol{k}$ and $\Delta_2\boldsymbol{k}$ are disjoint intervals, and $Z(\Delta_1\lambda + \Delta_2\lambda, \Delta\boldsymbol{k}) = Z(\Delta_1\lambda, \Delta\boldsymbol{k}) + Z(\Delta_2\lambda, \Delta\boldsymbol{k})$ if $\Delta_1\lambda$ and $\Delta_2\lambda$ are disjoint intervals;
3) $E\{Z(\Delta_1\lambda, \Delta_1\boldsymbol{k}) Z^*(\Delta_2\lambda, \Delta_2\boldsymbol{k})\} = 0$, if $\Delta_1\boldsymbol{k}$ and $\Delta_2\boldsymbol{k}$ are disjoint intervals, or if $\Delta_1\lambda$ and $\Delta_2\lambda$ are disjoint intervals;
4) $E\{|Z(\Delta\lambda, \Delta\boldsymbol{k})|^2\} = P(\lambda, \boldsymbol{k})(\Delta\lambda/2\pi)\, \Delta k_x \Delta k_y$,

where $P(\lambda, \boldsymbol{k})$ is the frequency-wavenumber power spectral density function and $2\pi k_x$, $2\pi k_y$ are the $x$, $y$ components, respectively, of the vector $\boldsymbol{k}$ in radians per kilometer. It should be noted that $Z(\Delta\lambda, \Delta\boldsymbol{k})$ is a random function with uncorrelated increments, where the increments can be taken either in frequency $\lambda$ or in vector wavenumber $\boldsymbol{k}$. The cross-covariance and cross-power spectral density can be written as

$$\rho(m, \boldsymbol{r}) = \int_{-\pi}^{\pi}\int_{-\infty}^{\infty}\int_{-\infty}^{\infty} P(\lambda, \boldsymbol{k}) \varepsilon^{-i(m\lambda + \boldsymbol{k}\cdot\boldsymbol{r})} \frac{d\lambda}{2\pi} dk_x dk_y \tag{7}$$

$$f(\lambda, \boldsymbol{r}) = \int_{-\infty}^{\infty}\int_{-\infty}^{\infty} P(\lambda, \boldsymbol{k}) \varepsilon^{-i\boldsymbol{k}\cdot\boldsymbol{r}} dk_x dk_y. \tag{8}$$

It is possible to write the frequency-wavenumber spectrum as

$$\begin{aligned} P(\lambda, \boldsymbol{k}) &= \sum_{m=-\infty}^{\infty}\int_{-\infty}^{\infty}\int_{-\infty}^{\infty} \rho(m, \boldsymbol{r}) \varepsilon^{i(m\lambda + \boldsymbol{k}\cdot\boldsymbol{r})} dr_x dr_y \\ &= \int_{-\infty}^{\infty}\int_{-\infty}^{\infty} f(\lambda, \boldsymbol{r}) \varepsilon^{i\boldsymbol{k}\cdot\boldsymbol{r}} dr_x dr_y, \end{aligned} \tag{9}$$

where $r_x$, $r_y$ are the $x$, $y$ components, respectively, of the vector $\boldsymbol{r}$, in kilometers.

If the signal consists of a unity amplitude monochromatic plane wave propagating with a velocity, $v_0$ km/s, of the form $\exp[-i(2\pi f_0 mT + \boldsymbol{k}_0 \cdot \boldsymbol{r})]$, $m = 0, \pm 1, \pm 2, \cdots$, where $f_0$ is the frequency, $T$ is the sampling period, $\boldsymbol{k}_0 = 2\pi f_0 \boldsymbol{\alpha}_0$, $-\boldsymbol{\alpha}_0$ is a slowness vector which points in the direction of propagation of the wave, and $|\alpha_0| = 1/v_0$, then

$$(2\pi)^{-1} f(\lambda, \boldsymbol{r}) = \exp[-i\boldsymbol{k}_0 \cdot \boldsymbol{r}]\delta(\lambda - \lambda_0)$$

and

$$\begin{aligned} (2\pi)^{-1} P(\lambda, \boldsymbol{k}) &= \int_{-\infty}^{\infty}\int_{-\infty}^{\infty} \delta(\lambda - \lambda_0) \exp[i(\boldsymbol{k} - \boldsymbol{k}_0)\cdot\boldsymbol{r}] dr_x dr_y \\ &= \delta(\lambda - \lambda_0, \boldsymbol{k} - \boldsymbol{k}_0) \end{aligned}$$

which is a delta function located at the frequency $\lambda_0 = 2\pi f_0 T$ and wavenumber $\boldsymbol{k}_0$. It should now be apparent how $P(\lambda, \boldsymbol{k})$ provides the information concerning the speed and azimuth, or vector velocity, of propagating waves.

## Conventional Method for Estimating Frequency-Wavenumber Spectrum

We now assume that $K$ sensors are to be used to estimate the frequency-wavenumber spectrum $P(\lambda, \boldsymbol{k})$. Such an estimate is usually based on an estimate for the cross-power spectral density $f_{jl}(\lambda)$. For simplicity, only the direct segment, or block averaging, method of estimation will be considered for estimating $f_{jl}(\lambda)$. It has been shown [3] that this method is very desirable from the point of view of computational efficiency. There is also no essential loss of generality in considering a specific estimation method for $f_{jl}(\lambda)$. In the direct segment method the number of data points $L$ in each channel is divided into $M$ nonoverlapping blocks of $N$ data points, $L = MN$. The Fourier transform of the data in the $n$th segment, $j$th channel, and normalized frequency $\lambda$, is

$$S_{jn}(\lambda) = (N)^{-1/2} \sum_{m=1}^{N} a_m N_{j,m+(n-1)N} \varepsilon^{im\lambda} \qquad \begin{matrix} j = 1, \cdots, K \\ n = 1, \cdots, M. \end{matrix} \tag{10}$$

The $a_m$ are weights which are used to control the shape of the frequency window used in estimating $f_{jl}(\lambda)$. Again, for simplicity, we assume $a_m = 1$, $m = 1, \cdots, N$. As an estimate for $f_{jl}(\lambda)$ we take

$$\hat{f}_{jl}(\lambda) = \frac{1}{M} \sum_{n=1}^{M} S_{jn}(\lambda) S_{ln}^*(\lambda), \qquad j, l = 1, \cdots, K. \tag{11}$$

We will assume hereafter that a normalization is performed by dividing $\hat{f}_{jl}(\lambda)$ by $[\hat{f}_{jj}(\lambda)\hat{f}_{ll}(\lambda)]^{1/2}$, in order to remove the effects of improper sensor equalization. We can, without any loss of generality, ignore this step in the ensuing analysis. As an estimate for $P(\lambda, \boldsymbol{k})$ we take

$$\hat{P}(\lambda, \boldsymbol{k}) = \frac{1}{K^2} \sum_{j,l=1}^{K} w_j w_l^* \hat{f}_{jl}(\lambda) \varepsilon^{i\boldsymbol{k}\cdot(\boldsymbol{x}_j - \boldsymbol{x}_l)} \tag{12}$$

where the $w_j$ are weights which are used to control the shape of the wavenumber window used in estimating $P(\lambda, \boldsymbol{k})$. We will assume, for simplicity, that $w_j = 1$, $j = 1, \cdots, K$. It has been shown that $\{\hat{f}_{jl}(\lambda)\}$ is a nonnegative-definite matrix so that $\hat{P}(\lambda, \boldsymbol{k})$ will be real and nonnegative [3].

It will now be shown that $\hat{P}$ is an asymptotically unbiased and consistent estimate for $cP$ where $c$ is some positive constant. Using the results of [3] for $E\{\hat{f}_{jl}(\lambda)\}$ we get

$$\begin{aligned} E\{\hat{P}(\lambda, \boldsymbol{k}_0)\} = \int_{-\pi}^{\pi}\int_{-\infty}^{\infty}\int_{-\infty}^{\infty} & P(x, \boldsymbol{k}) |B(\boldsymbol{k} - \boldsymbol{k}_0)|^2 \\ & \cdot |W_N(x - \lambda)|^2 \frac{dx}{2\pi} dk_x dk_y \end{aligned} \tag{13}$$

where $|W_N(x)|^2$ is the Bartlett window

$$|W_N(x)|^2 = \frac{1}{N}\left|\frac{\sin(N/2)x}{\sin(1/2)x}\right|^2, \tag{14}$$

and $|B(\boldsymbol{k})|^2$ is the beamforming array response pattern

$$B(\boldsymbol{k}) = \frac{1}{K}\sum_{j=1}^{K} \varepsilon^{i\boldsymbol{k}\cdot\boldsymbol{x}_j}. \tag{15}$$

Thus, $E\{\hat{P}(\lambda, \boldsymbol{k}_0)\}$ is obtained by means of a frequency-wavenumber window $|W_N(x-\lambda)|^2 \cdot |B(\boldsymbol{k}-\boldsymbol{k}_0)|^2$. Hence, $\hat{P}$ will be an asymptotically unbiased estimate for $cP$ if $|W_N(x-\lambda)\cdot B(\boldsymbol{k}-\boldsymbol{k}_0)|^2$ approaches a delta function in such a way that

$$\int_{-\pi}^{\pi}\int_{-\infty}^{\infty}\int_{-\infty}^{\infty} |W_N(x-\lambda)\cdot B(\boldsymbol{k}-\boldsymbol{k}_0)|^2 \frac{dx}{2\pi}\,dk_x dk_y = c.$$

Using the results of [3] we can compute the variance of $\hat{P}$ as, assuming $\{N_{jm}\}$ is a multidimensional Gaussian process,

$$\begin{aligned}\mathrm{VAR}\,\{\hat{P}(\lambda, \boldsymbol{k}_0)\} = {} & \frac{1}{M}\{E[\hat{P}(\lambda, \boldsymbol{k}_0)]\}^2 \\ & + \frac{1}{M}\left|\int_{-\pi}^{\pi}\int_{-\infty}^{\infty}\int_{-\infty}^{\infty} \cdot P(x, \boldsymbol{k})B^*(\boldsymbol{k}-\boldsymbol{k}_0)B(\boldsymbol{k}+\boldsymbol{k}_0) \right. \\ & \left. \cdot |W_N(x-\lambda)|^2 \frac{dx}{2\pi}\,dk_x dk_y\right|^2.\end{aligned}$$

Thus,

$$\begin{aligned}\mathrm{VAR}\,\{\hat{P}(\lambda, \boldsymbol{k}_0)\} &\cong \frac{1}{M}\{E[\hat{P}(\lambda, \boldsymbol{k}_0)]\}^2, \qquad |\boldsymbol{k}_0| \neq 0 \\ &= \frac{2}{M}\{E[\hat{P}(\lambda, \boldsymbol{k}_0)]\}^2, \qquad |\boldsymbol{k}_0| = 0.\end{aligned} \tag{16}$$

Since the variance of $\hat{P}$ approaches zero as $M$ approaches infinity, it follows that $\hat{P}$ is a consistent estimate for $cP$.

We follow Blackman and Tukey [4] and assume that $\hat{P}(\lambda, \boldsymbol{k}_0)$ is a multiple of a chi-square variable so that to establish confidence intervals the chi-square distribution can be used with the number of degrees of freedom $k$ given by

$$\begin{aligned}k &= 2\{E[\hat{P}(\lambda, \boldsymbol{k}_0)]\}^2/\mathrm{VAR}\,[\hat{P}(\lambda, \boldsymbol{k}_0)] \\ &= 2M, |\boldsymbol{k}_0| \neq 0 \\ &= M, |\boldsymbol{k}_0| = 0,\end{aligned} \tag{17}$$

if $M=36$, $k=72$, and the 90 percent confidence limits are approximately $\pm 1.2$ dB, and if $|\boldsymbol{k}_0| \neq 0$. When $|\boldsymbol{k}_0|=0$, these limits are approximately $\pm 1.6$ dB.

## High-Resolution Method for Estimating Frequency-Wavenumber Spectrum

The high-resolution estimate for $P(\lambda, \boldsymbol{k})$ is defined as

$$P'(\lambda, \boldsymbol{k}) = \left[\sum_{j,l=1}^{K} \hat{q}_{jl}(\lambda)\exp\left[i\boldsymbol{k}\cdot(\boldsymbol{x}_j - \boldsymbol{x}_l)\right]\right]^{-1} \tag{18}$$

where $\{\hat{q}_{jl}(\lambda)\}$ is the inverse of the spectral matrix $\{\hat{f}_{jl}(\lambda)\}$. The motivation for this procedure can be given by writing (18) as

$$\begin{aligned}P'(\lambda, \boldsymbol{k}) &= \sum_{j,l=1}^{K} A_j^*(\lambda, \boldsymbol{k})A_l(\lambda, \boldsymbol{k})\hat{f}_{jl}(\lambda)\exp\left[i\boldsymbol{k}\cdot(\boldsymbol{x}_j - \boldsymbol{x}_l)\right] \\ &= \frac{1}{M}\sum_{n=1}^{M}\left|\sum_{j=1}^{K} A_j^*(\lambda, \boldsymbol{k})S_{jn}(\lambda)\exp\left[i\boldsymbol{k}\cdot\boldsymbol{x}_j\right]\right|^2\end{aligned} \tag{19}$$

where

$$A_j(\lambda, \boldsymbol{k}) = \frac{\sum_{l=1}^{K} q_{jl}(\lambda, \boldsymbol{k})}{\sum_{j,l=1}^{K} q_{jl}(\lambda, \boldsymbol{k})} \tag{20}$$

and $\{q_{ij}(\lambda, \boldsymbol{k})\}$ is the inverse of the matrix $\{\exp\left[i\boldsymbol{k}\cdot(\boldsymbol{x}_j - \boldsymbol{x}_l)\right]\hat{f}_{jl}(\lambda)\}$. Thus, $P'(\lambda, \boldsymbol{k}_0)$ is the power output of an array processor, known as a maximum-likelihood filter, whose design is determined by the sensor data and is different for each wavenumber $\boldsymbol{k}_0$, which passes undistorted any monochromatic plane wave traveling at a velocity corresponding to the wavenumber $\boldsymbol{k}_0$ and suppresses in an optimum least-squares sense the power of those waves traveling at velocities corresponding to wavenumbers other than $\boldsymbol{k}_0$, cf. [3, (122) and (123)]. It should be noted that the amount of computation required to obtain $P'$ is almost the same as that to get $\hat{P}$, since only an additional Hermitian matrix inversion is required.

We now wish to compute the mean and variance of $P'$. In order to do this we assume that $M$, $N$ are large enough so that as an approximation we may replace $\hat{f}_{jl}(\lambda)$ by $f_{jl}(\lambda)$ in the definition for $A_j(\lambda, \boldsymbol{k})$ in (20). This then implies that the weights $A_j(\lambda, \boldsymbol{k})$ are not random and can be replaced by their expected values. This is a simplifying assumption, which is not actually valid, since these weights are designed from the data. However, it does appear to be a reasonable approximation. Using this assumption we have

$$\begin{aligned}E\{P'(\lambda, \boldsymbol{k}_0)\} = {} & \int_{-\pi}^{\pi}\int_{-\infty}^{\infty}\int_{-\infty}^{\infty} P(x, \boldsymbol{k})|W_N(x-\lambda) \\ & \cdot B'(\lambda, \boldsymbol{k}, \boldsymbol{k}_0)|^2 \frac{dx}{2\pi}\,dk_x dk_y\end{aligned} \tag{21}$$

where

$$B'(\lambda, \boldsymbol{k}, \boldsymbol{k}_0) = \sum_{j=1}^{K} A_j(\lambda, \boldsymbol{k}_0)\exp\left[i(\boldsymbol{k}-\boldsymbol{k}_0)\cdot\boldsymbol{x}_j\right]. \tag{22}$$

It should be noted that the functional form, or shape, of $B'$ changes as a function of the wavenumber $\boldsymbol{k}_0$. Thus, $E\{P'(\lambda, \boldsymbol{k}_0)\}$ is obtained by means of a frequency-wavenumber window $|W_N(x-\lambda)\cdot B'(\lambda, \boldsymbol{k}, \boldsymbol{k}_0)|^2$. Hence, $P'$ will be an asymptotically unbiased estimate for $cP$ if $|W_N(x-\lambda)\cdot B'(\lambda, \boldsymbol{k}, \boldsymbol{k}_0)|^2$ approaches a 3-dimensional delta function in such a way that

$$\int_{-\pi}^{\pi}\int_{-\infty}^{\infty}\int_{-\infty}^{\infty} |W_N(x-\lambda)\cdot B'(\lambda, \boldsymbol{k}, \boldsymbol{k}_0)|^2 \frac{dx}{2\pi}\,dk_x dk_y = c \tag{23}$$

where $c$ is some positive number.

The variance of $P'$ is, assuming $\{N_{jm}\}$ is a multidimensional Gaussian process,

$$\begin{aligned}\text{VAR}\{P'(\lambda, \boldsymbol{k}_0)\} = \frac{1}{M}\{E[P'(\lambda, \boldsymbol{k}_0)]\}^2 + \frac{1}{M}\Big|\int_{-\pi}^{\pi}\int_{-\infty}^{\infty}\int_{-\infty}^{\infty} \\ \cdot P(x, \boldsymbol{k})B'^*(\lambda, \boldsymbol{k}, \boldsymbol{k}_0)B'(\lambda, \boldsymbol{k}, -\boldsymbol{k}_0) \\ \cdot |W_N(x-\lambda)|^2 \frac{dx}{2\pi} dk_x dk_y.\end{aligned} \tag{24}$$

Thus,

$$\begin{aligned}\text{VAR}\{P'(\lambda, \boldsymbol{k}_0)\} &\cong \frac{1}{M}\{E[P'(\lambda, \boldsymbol{k}_0)]\}^2, \qquad |\boldsymbol{k}_0| \neq 0 \\ &= \frac{2}{M}\{E[P'(\lambda, \boldsymbol{k}_0)]\}^2, \qquad |\boldsymbol{k}_0| = 0.\end{aligned} \tag{25}$$

The confidence limits for $P'$ can be obtained in a manner similar to that for $\hat{P}$ described previously.

It will now be shown that the wavenumber resolution using $P'$ is higher than that obtained by using $\hat{P}$. We assume that a single plane wave is propagating across the array of sensors and that a noise component is present in each sensor which is incoherent between any pair of sensors. If $M, N$ are large, then the spectral matrix is given by

$$\hat{f}_{jl}(\lambda_0) = \delta_{jl}(R)\exp[-i\boldsymbol{k}_0\cdot(\boldsymbol{x}_j - \boldsymbol{x}_l)], \quad j, l = 1, \cdots, K \tag{26}$$

where

$$\begin{aligned}\delta_{jl}(R) &= 1, \qquad j = l \\ &= 1 - R, \qquad j \neq l\end{aligned} \tag{27}$$

$R$ is the ratio of the incoherent noise power to the total power of the sensor output, $\boldsymbol{k}_0 = 2\pi f_0 \boldsymbol{\alpha}$, $f_0$ is the frequency, $\lambda_0 = 2\pi f_0 T$, $T$ is the sampling period, $-\boldsymbol{\alpha}$ is the slowness vector which points in the direction of propagation and has magnitude $|\alpha| = 1/v$, $v$ is the phase velocity of the propagating wave. Hence, using (12) we have

$$\hat{P}(\lambda_0, \boldsymbol{k}) = (1-R)|B(\Delta\boldsymbol{k}_0)|^2 + \frac{R}{K} \tag{28}$$

where

$$\Delta\boldsymbol{k}_0 = \boldsymbol{k} - \boldsymbol{k}_0. \tag{29}$$

If we denote the matrix given in (26) by $F$, then

$$F = (1-R)\left[q'q + \frac{R}{1-R}I\right], \tag{30}$$

where $I$ is the $K \times K$ identity matrix, $q$ is a $1 \times K$ row matrix whose 1 $j$th element is $\exp[i\boldsymbol{k}_0\cdot\boldsymbol{x}_j]$ and $q'$ is a $K \times 1$ column matrix whose $j$ 1th element is $\exp[-i\boldsymbol{k}_0\cdot\boldsymbol{x}_j]$. Now we have the following matrix inversion formula

$$\left[(1-R)\left(q'q + \frac{R}{1-R}I\right)\right]^{-1} = \frac{1}{R}\left[I - \frac{q'q}{K + \frac{R}{1-R}}\right], \tag{31}$$

so that using (18) we have

$$P'(\lambda_0, \boldsymbol{k}) = \frac{R}{K}\frac{1 - R + (R/K)}{1 - R + 2(R/K) - \hat{P}(\lambda_0, \boldsymbol{k})}. \tag{32}$$

If $\boldsymbol{k} = \boldsymbol{k}_0$, then

$$\hat{P}(\lambda_0, \boldsymbol{k}_0) = P'(\lambda_0, \boldsymbol{k}_0) = 1 - R + \frac{R}{K}. \tag{33}$$

In the vicinity of $\boldsymbol{k} = \boldsymbol{k}_0$ we consider that power contour, or those values of $\boldsymbol{k}$, for which $\hat{P}(\lambda_0, \boldsymbol{k}) = 1 - R$, which is still very close to the peak value of $1 - R + (R/K)$, since $R$ is small, between zero and unity, and $K$ is large, usually about 20. For these values of $\boldsymbol{k}$ we get $P'(\lambda_0, \boldsymbol{k}) = \frac{1}{2}(1 - R + R/K)$, so that $P'$ is already 3 dB down from its peak value of $1 - R + R/K$. Hence, the wavenumber resolution using $P'$ will be much higher than that obtained with $\hat{P}$.

We now assume that there are two independent and random plane waves propagating across the array of sensors, plus incoherent noise, so that the spectral matrix is

$$F = q_1'q_1 + q_2'q_2 + RI \tag{34}$$

where $q_1$, $q_2$ are $1 \times K$ row matrices whose 1 $j$th elements are, respectively, $b_1 \exp[i\boldsymbol{k}_1\cdot\boldsymbol{x}_j]$ and $b_2 \exp[i\boldsymbol{k}_2\cdot\boldsymbol{x}_j]$, and $b_1^2 + b_2^2 + R = 1$. We now have

$$\hat{P}(\lambda_0, \boldsymbol{k}) = \sum_{j=1}^{2} b_j^2 |B(\Delta\boldsymbol{k}_j)|^2 + \frac{R}{K}, \tag{35}$$

where $\Delta\boldsymbol{k}_j = \boldsymbol{k} - \boldsymbol{k}_j$.

In order to find an expression for $P'(\lambda, \boldsymbol{k})$ we note the following matrix inversion formula

$$\begin{aligned}[(RI + q_1'q_1) + q_2'q_2]^{-1} &= (RI + q_1'q_1)^{-1} \\ &\quad + \frac{(RI + q_1'q_1)^{-1}q_2'q_2(RI + q_1'q_1)^{-1}}{1 + q_2(RI + q_1'q_1)^{-1}q_2'}.\end{aligned} \tag{36}$$

Using this formula, as well as that given in (31) we obtain

$$\begin{aligned}[P'(\lambda_0, \boldsymbol{k})]^{-1} &= [P_1'(\lambda_0, \boldsymbol{k})]^{-1} - \left(\frac{K}{R}\right)^2 \\ &\cdot \left[\frac{b_2^2|B(\Delta\boldsymbol{k}_2)|^2 - \frac{2Kb_1^2b_2^2}{R + Kb_1^2}\text{Re}\{B(\Delta\boldsymbol{k}_1)B(\Delta\boldsymbol{k}_{12})B^*(\Delta\boldsymbol{k}_2)\} + b_1^4b_2^2|B(\Delta\boldsymbol{k}_1)B(\Delta\boldsymbol{k}_{21})|^2\frac{K^2}{(R + Kb_1^2)^2}}{1 + \frac{K}{R}\left(b_2^2 - \frac{Kb_1^2b_2^2|B(\Delta\boldsymbol{k}_{21})|^2}{R + Kb_1^2}\right)}\right]\end{aligned} \tag{37}$$

where $\Delta\boldsymbol{k}_{jl} = \boldsymbol{k}_j - \boldsymbol{k}_l$ and

$$P_j'(\lambda_0, \boldsymbol{k}) = \frac{R}{K}\frac{b_j^2 + \frac{R}{K}}{b_j^2 + \frac{2R}{K} - \hat{P}_j(\lambda_0, \boldsymbol{k})}, \qquad j = 1, 2, \tag{38}$$

$$\hat{P}_j(\lambda_0, \boldsymbol{k}) = b_j^2|B(\Delta \boldsymbol{k}_j)|^2 + \frac{R}{K}, \qquad j = 1, 2. \tag{39}$$

Thus $P_j'$ is the high-resolution frequency-wavenumber spectrum obtained when only the $j$th propagating wave, plus incoherent noise, is present. In the vicinity of $\boldsymbol{k} = \boldsymbol{k}_1$ we would like $P' \cong P_1'$. Hence, the second term in (37) represents an undesired error term in this region which we would like to be as small as possible. It can easily be shown that this error term will be small compared to $1/P_1'$ if

$$b_2^2[R + Kb_1^2(1 - |B(\Delta \boldsymbol{k}_{12})|^2)] \gg R|B(\Delta \boldsymbol{k}_{12})|^2 b_2^2 - \frac{R}{K}(R + Kb_1^2). \tag{40}$$

In most cases $R/K$ will be very small so that we may write (40) as

$$b_1^2 \gg \frac{R}{K} \frac{|B(\Delta \boldsymbol{k}_{12})|^2}{1 - |B(\Delta \boldsymbol{k}_{12})|^2}. \tag{41}$$

This inequality will be satisfied if either $R/K$ is small, $|B(\Delta \boldsymbol{k}_{12})|^2$ is small or both of these quantities are small. It should be noted that $|B(\Delta \boldsymbol{k}_{12})|^2$ will be small if the wavenumber $\boldsymbol{k}_1$ corresponding to one of the propagating waves is sufficiently different from the wavenumber $\boldsymbol{k}_2$ of the other propagating wave. In this case the two propagating waves can be resolved in wavenumber by the natural beam pattern of the array of sensors, $|B(\boldsymbol{k})|^2$. However, if $|B(\Delta \boldsymbol{k}_{12})|^2$ is not too small, so that the natural beam pattern can not resolve the two waves, it is still possible for the high-resolution method to resolve the two waves if $R/K$ is small and $|B(\Delta \boldsymbol{k}_{12})|^2 < 1$. Thus, we see the advantage of the high-resolution method over the conventional method of frequency-wavenumber spectrum analysis. In a similar manner we may show that in the vicinity of $\boldsymbol{k} = \boldsymbol{k}_2$, $P' \cong P_2$ if

$$b_2^2 \gg \frac{R}{K} \frac{|B(\Delta \boldsymbol{k}_{21})|^2}{1 - |B(\Delta \boldsymbol{k}_{21})|^2}. \tag{42}$$

Thus, we have shown that a certain type of linearity holds, i.e.,

$$P'(\lambda_0, \boldsymbol{k}) \cong \sum_{j=1}^{2} P_j'(\lambda_0, \boldsymbol{k}). \tag{43}$$

In other words, the high-resolution spectrum of the sum of two propagating waves, plus a small amount of incoherent noise, is the sum of the high-resolution spectra for the individual waves, as indicated in (43). This result may be extended to the case of $M$ propagating waves, but the precise conditions for the linearity to hold become cumbersome to derive. It has been found experimentally that linearity will hold if there is sufficient wavenumber separation between the propagating waves and if the beam pattern $|B(\boldsymbol{k})|^2$ is reasonably good.

The high-resolution estimate is based on the inverse of the estimated spectral matrix, cf. (18). Therefore, the problem of whether this inverse exists is extremely important. As mentioned previously, it has been shown that $\{\hat{f}_{jl}(\lambda)\}$ is a non-negative-definite matrix when the block averaging method of spectral estimation is used [3]. However, this is not good enough to insure that the inverse of the spectral matrix exists. That is, it must be shown that the spectral matrix is positive-definite in order that its inverse exist.

In fact, if the number of blocks $M$ is less than the number of sensors $K$, then the spectral matrix is of order $K$, but only of rank $M$ at most and is thus singular. This can be seen by writing the spectral matrix $F$ as

$$F = \sum_{n=1}^{M} q_n' q_n \tag{44}$$

where $q_n$ is a $1 \times K$ row matrix whose 1 $j$th element is

$$\sum_{m=1}^{N} N_{j,m+(n-1)N} e^{im\lambda}.$$

Thus, $F$ is the sum of $M$ matrices each having rank unity, and the rank of $F$ cannot exceed the sum of the ranks, namely $M$. Hence, $F$ has rank $M$ at most and, if $M < K$, $F$ must be singular. Therefore, a necessary, but not sufficient, condition for $F$ to be nonsingular is $M \geq K$. As a practical matter, it is found that whenever $M \geq K$, $F$ will be nonsingular, providing there is reasonable data in each block.

However, in some cases it is not possible to obtain $K$ or more data blocks. This situation arises, for example, when analysis of transient signals is desired whose time duration, unlike that of the noise, is very short. In order to make the spectral matrix nonsingular a small amount of incoherent noise is added. This is accomplished by modifying the matrix $F$ given in (44) into the matrix $F'$ given by

$$F' = (1 - R)F + RI. \tag{45}$$

We now show that $F'$ is positive definite, and thus nonsingular.

Consider the quadratic form $Q$ associated with the matrix $F'$

$$\begin{aligned} Q &= \sum_{j=1}^{K} \sum_{l=1}^{K} a_j a_l^* \hat{f}_{jl}(\lambda) \\ &= \frac{1 - R}{L} \sum_{n=1}^{M} \left| \sum_{j=1}^{K} \sum_{m=1}^{M} a_j N_{j,m+(n-1)N} e^{im\lambda} \right|^2 \\ &\quad + R \sum_{j=1}^{K} |a_j|^2, \qquad -\pi \leq \lambda \leq \pi. \end{aligned} \tag{46}$$

Now, if $Q = 0$, we must have

$$\sum_{j=1}^{K} |a_j|^2 = 0, \tag{47}$$

since the first term in (46) is always nonnegative. However, (47) implies that $a_j = 0$, $j = 1, \cdots, K$, which proves that $F'$ is positive definite.

## Applications to Seismic Data

We now wish to describe the application of the conventional and high-resolution frequency-wavenumber spectrum estimates to seismic data obtained from LASA. The

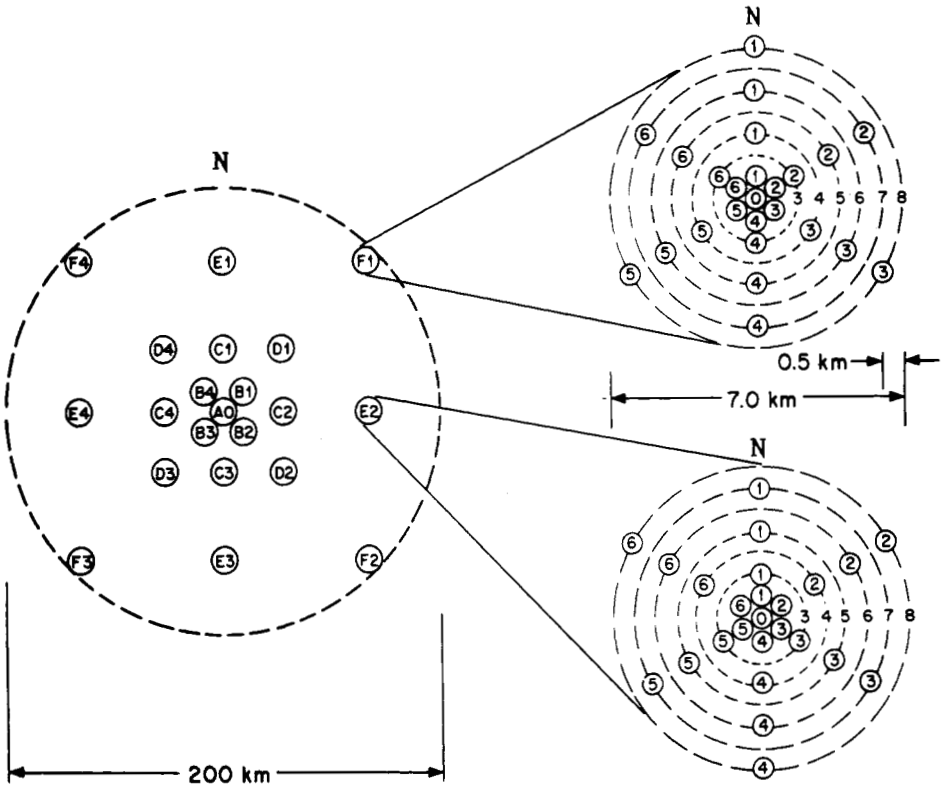


Fig. 1. General arrangement of the large aperture seismic array.

TABLE I

PARAMETERS USED IN MEASUREMENT OF FREQUENCY-WAVENUMBER SPECTRUM

| DATA | Sampling Rate (Hz) | Array Aperture (km) | Nominal Number of Sensors = $K$ | Number of Samples per Block = $N$ | Frequency Resolution (Hz) | Number of Blocks = $M$ | 90% Confidence Limits (dB) | Added Amount Incoherent Noise = $R$ |
|---|---|---|---|---|---|---|---|---|
| LPZ noise | 1 | 200 | 21 | 100 | 0.01 | 36 | ±1.2 | 0 |
| LPZ Rayleigh surface-wave event (entire wave) | 1 | 200 | 21 | 100 | 0.01 | 36 | — | 0 |
| LPZ Rayleigh surface-wave event (200 seconds at a time) | 1 | 200 | 21 | 100 | 0.01 | 2 | — | 0.05 |
| SP noise | 10 | 36 | 25 | 100 | 0.10 | 36 | ±1.2 | 0 |

LASA consists of 21 subarrays of 25 short-period (SP) vertical seismometers as indicated in Fig. 1. At the center of each subarray there is a three-component set of long-period (LP) seismometers oriented in the vertical (Z), north–south (NS), and east–west (EW) directions.

As mentioned previously, a direct segment, or block averaging, method of spectral estimation was employed. The weights $a_j = 1$, $j = 1, \cdots, N$ were used, cf. (10) so that a Bartlett frequency window was used in the spectral estimation [4]. The seismic data considered was LPZ noise, LPZ Rayleigh surface-wave events, and SP noise. The parameters used in the measurement are given in Table I. The results of the conventional frequency-wavenumber spectrum measurement program are displayed, at a fixed frequency, as contours of $-10 \log [\hat{P}(\lambda, \boldsymbol{k})/\hat{P}_{\max}]$ vs $k_x$, $k_y$, where $\hat{P}_{\max}$ is the maximum value of $\hat{P}$. The wavenumber coordinates are in cycles per kilometer. The wavenumber grid on which $\hat{P}$ is computed consists of $61 \times 61$ points. The level of the contours varies from 0 to 12 dB in steps of 1 dB. The display of the high-resolution results is similar to that of the conventional results with the only exception that the contour levels are incremented by 2 dB. It should be noted that if a wave is propagating from the north with a velocity corresponding to the wavenumber $\boldsymbol{k}_0$, then the wavenumber spectrum results will show a peak at the point $k_x = 0$, $k_y = |\boldsymbol{k}_0|/2\pi$, i.e., the peak will appear above the origin of the wavenumber axes.

The transfer function of the LP system is shown in Fig. 2. The results of both the conventional and high-resolution frequency-wavenumber spectrum measurements for LPZ

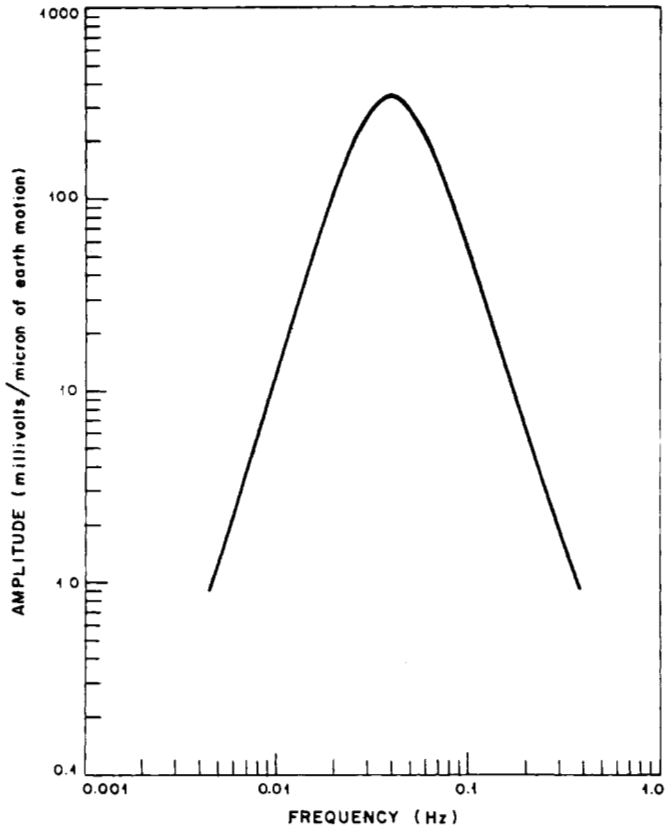


Fig. 2. Long-period system transfer function.

noise are shown in Figs. 3 and 4 for two different noise samples taken on 7 April 1967 and 26 January 1967, respectively. These figures show that the conventional and high-resolution results are in agreement as both methods tend to show strong peaks occurring at the same wavenumber in each program. However, the high-resolution method delineates the frequency-wavenumber spectrum much more clearly than the conventional method, especially in the suppression of the sidelobe level. This is demonstrated quite well in Fig. 4 which shows a 360° azimuthal spread for the wavenumber structure with a variable power density along this circle. This is, of course, exactly what would be expected since the dispersion curve of the LPZ propagating seismic noise has been measured and found to correspond to that of a fundamental mode Rayleigh wave [5]. This implies that at a given period the phase velocity of the propagating noise at LASA must be constant, independent of the location of the sources of the noise, and thus its frequency-wavenumber spectrum must consist of an arc, or arcs, whose extent corresponds to the range of the azimuths of the noise sources.

The results of Fig. 3 show the noise consists essentially of a single wave propagating from the north. In this case the conventional result should appear essentially the same as the beam pattern of LASA, with the peak of the beam pattern occurring at the wavenumber corresponding to the vector velocity of the propagating wave. That this is indeed the case can be seen by comparing Fig. 3 with Fig. 5 which shows the beam pattern of LASA. It should be noted that frequency-wavenumber spectra were computed for a theoretical model of the LPZ noise and showed excellent agreement with the measurements obtained using the actual LPZ seismic noise data. We also mention that the computer running time to produce a pair of plots, such as is shown in Fig. 3, is approximately 10 minutes using the IBM 360/67.

Another application of interest is to LPZ Rayleigh surface-wave events. In this case the propagating waves are transients, in time, and the field of sensor outputs cannot be considered as a homogeneous random field, as is the case with propagating seismic noise waves. Therefore, the frequency-wavenumber spectrum must be redefined in this case. Towards this end consider the time correlation function

$$\rho_{jl}(m) = \underset{A\to\infty}{\text{LIMIT}} \frac{T}{2A} \sum_{n=-A}^{A} N_{j,n} N_{l,n-m}.$$

The spectral densities $f_{jl}(\lambda)$, $f(\lambda, \boldsymbol{r})$ are defined in the same manner as previously, cf. (2), (4), respectively, and the frequency-wavenumber spectral density $P(\lambda, \boldsymbol{k})$ is also defined as previously in (9). The measurement of $P(\lambda, \boldsymbol{k})$ is still done by the direct segment method as indicated in (12) and (18). This represents an approximation which produces reasonable results.

The frequency-wavenumber spectrum was measured for the 21 November 1966 Kurile Islands event whose param-

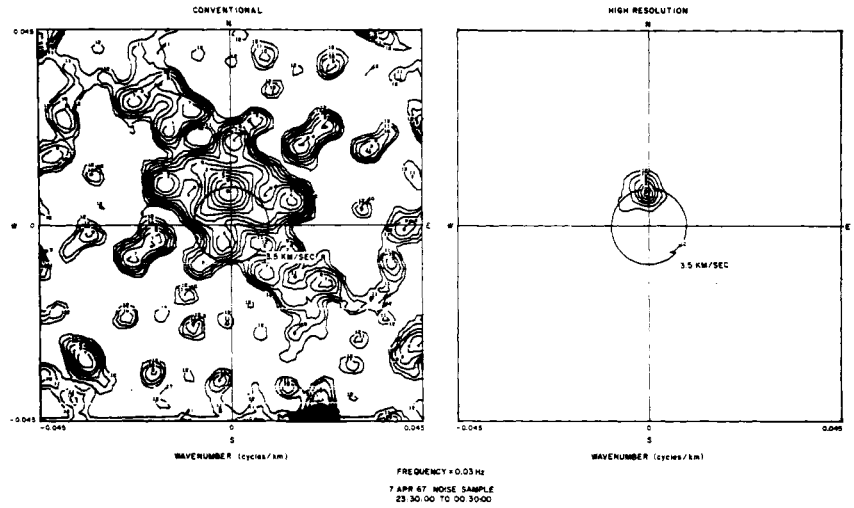


Fig. 3. Conventional and high-resolution frequency-wavenumber spectra for 7 April 1967 long-period noise sample.

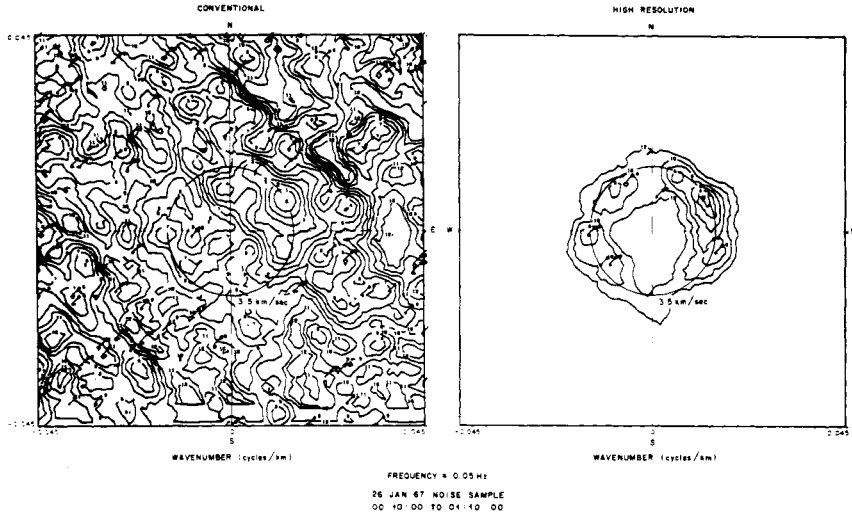


Fig. 4. Conventional and high-resolution frequency-wavenumber spectra for 26 January 1967 long-period noise sample.

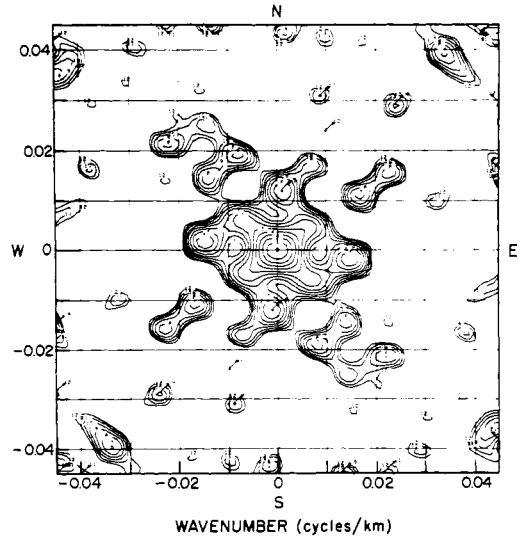


Fig. 5. The beam pattern for the large aperture seismic array.

TABLE II

PARAMETERS FOR 21 NOVEMBER 1966 KURILE ISLANDS EVENT

| | |
|---|---|
| Date: | 21 November 1966 |
| Region: | Kurile Islands |
| Origin time: | 12:19:27 |
| Latitude: | 46.7 N |
| Longitude: | 152.5 E |
| Distance: | 64.3° |
| Azimuth: | 312° |
| Depth: | 40 km |
| Body-Wave Magnitude: | 6.0 |

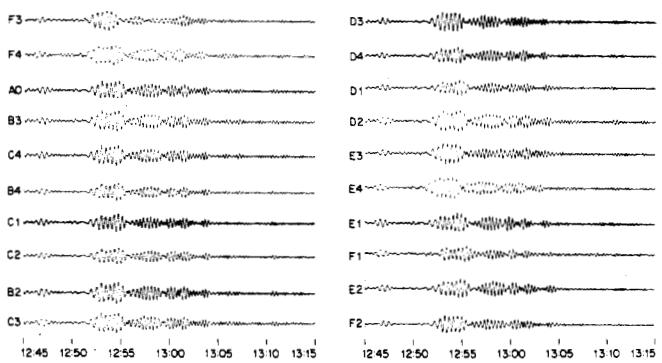


Fig. 6. The long-period waveforms for 21 November 1966 Kurile Islands event.

eters are given in Table II. The LPZ Rayleigh surface waves of this event are shown in Fig. 6. The results obtained by measuring the frequency-wavenumber spectrum over the entire LPZ Rayleigh surface-wave train, as indicated in Table I, are given in Fig. 7 for frequencies of 0.03, 0.04, 0.05 Hz. It is known that the beating, or modulation, of the envelope of these surface waves, as shown in Fig. 6, is caused by multiple path propagation, especially at shorter periods, cf. [6]–[8]. This multipath propagation effect is shown quite clearly at 0.04 Hz where two peaks are resolvable. One peak is at an azimuth corresponding to the initial wave arriving along the great circle path between LASA and the Kurile Islands, while the other peak shows the later multipath arrival propagating from the northwest.

In order to determine the time delay between the multipath arrivals at LASA, for the 25-second period group, the frequency-wavenumber spectrum was measured over successive 200-second-long blocks of time, as indicated in Table I. The results are given in Fig. 8, which, for simplicity, shows only the high-resolution results. Fig. 8(a) shows that the initial 25-second period group arrives from approximately the azimuth of the event, while Figs. 8(b)–(d) show the later arrivals coming from a more northerly direction. The time delay between the multipath arrivals appears to be about 200 seconds, since the emergence of a secondary peak to the north is visible in Fig. 8(b). The group velocity for these waves at the 25-second period is about 3.3 km/s so that a path length difference of about 660 km or 6 degrees

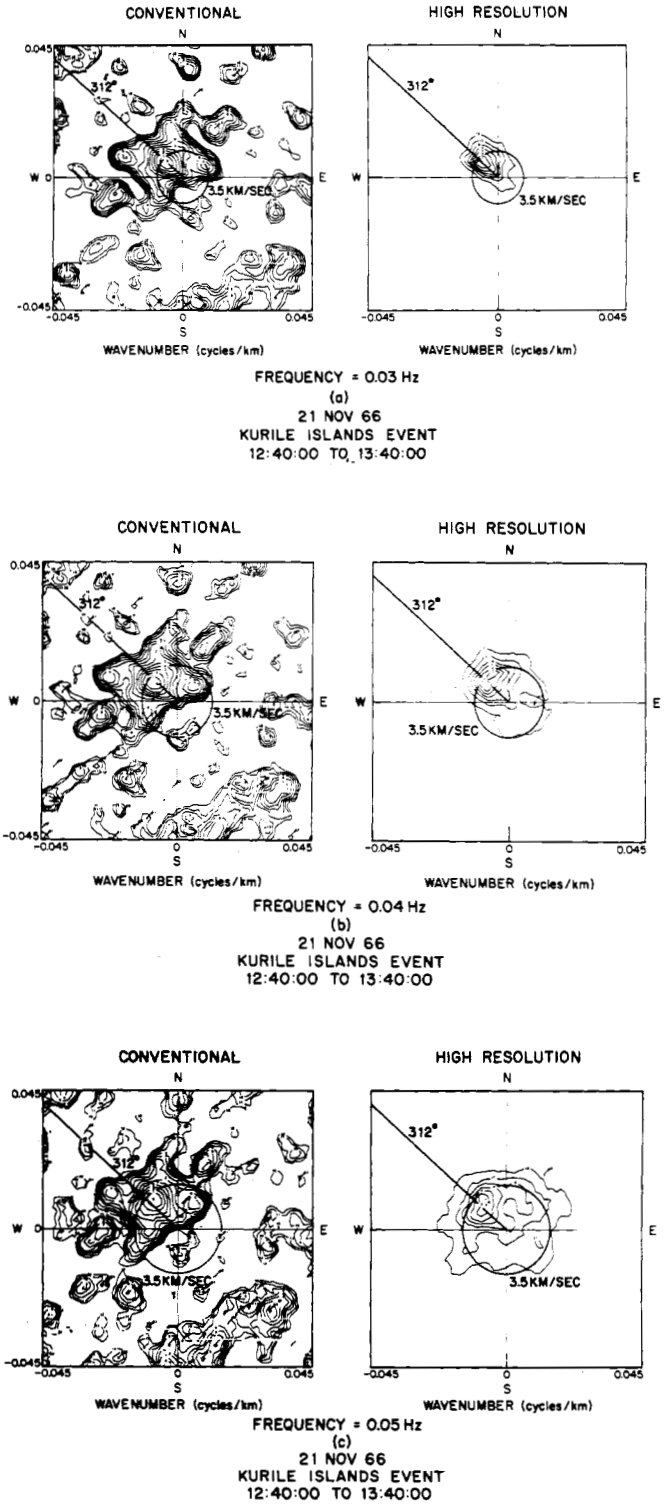


Fig. 7. Conventional and high-resolution frequency-wavenumber spectra for 21 November 1966 Kurile Islands event: 12:40:00 to 13:40:00. (a) Frequency = 0.03 Hz. (b) Frequency = 0.04 Hz. (c) Frequency = 0.05 Hz.

exists between the two multipath arrivals. Similar results have been obtained by Evernden by measuring phase velocities with a tripartite array [7], [8]. In addition, Evernden gives a theory to explain the causes of the multipath propagation of Rayleigh surface waves.

We now discuss the application of our results to SP noise. The transfer function of the SP system is shown in Fig. 9.

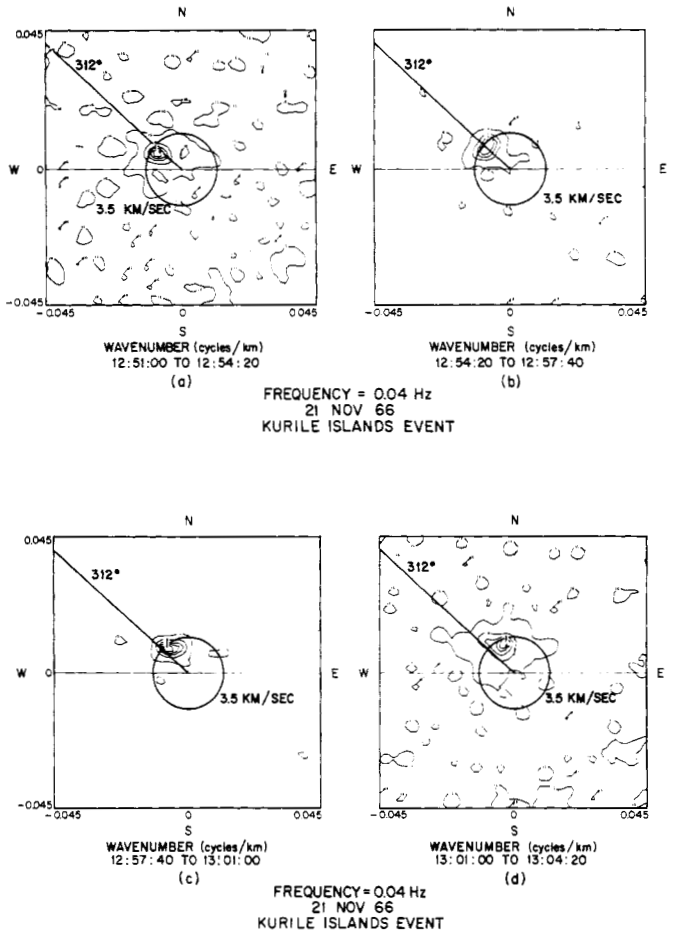


Fig. 8. Conventional and high-resolution frequency-wavenumber spectra for successive 200 second intervals of 21 November 1966 Kurile Islands event. Frequency = 0.04 Hz. Wavenumber (cycles/km) (a) 12:51:00 to 12:54:20. (b) 12:54:20 to 12:57:40 (c) 12:57:40 to 13:01:00 (d) 13:01:00 to 13:04:20.

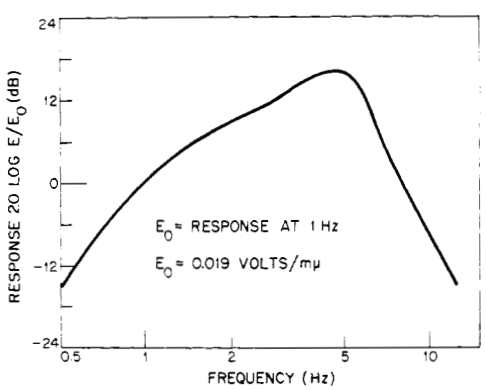


Fig. 9. Short-period system transfer function.

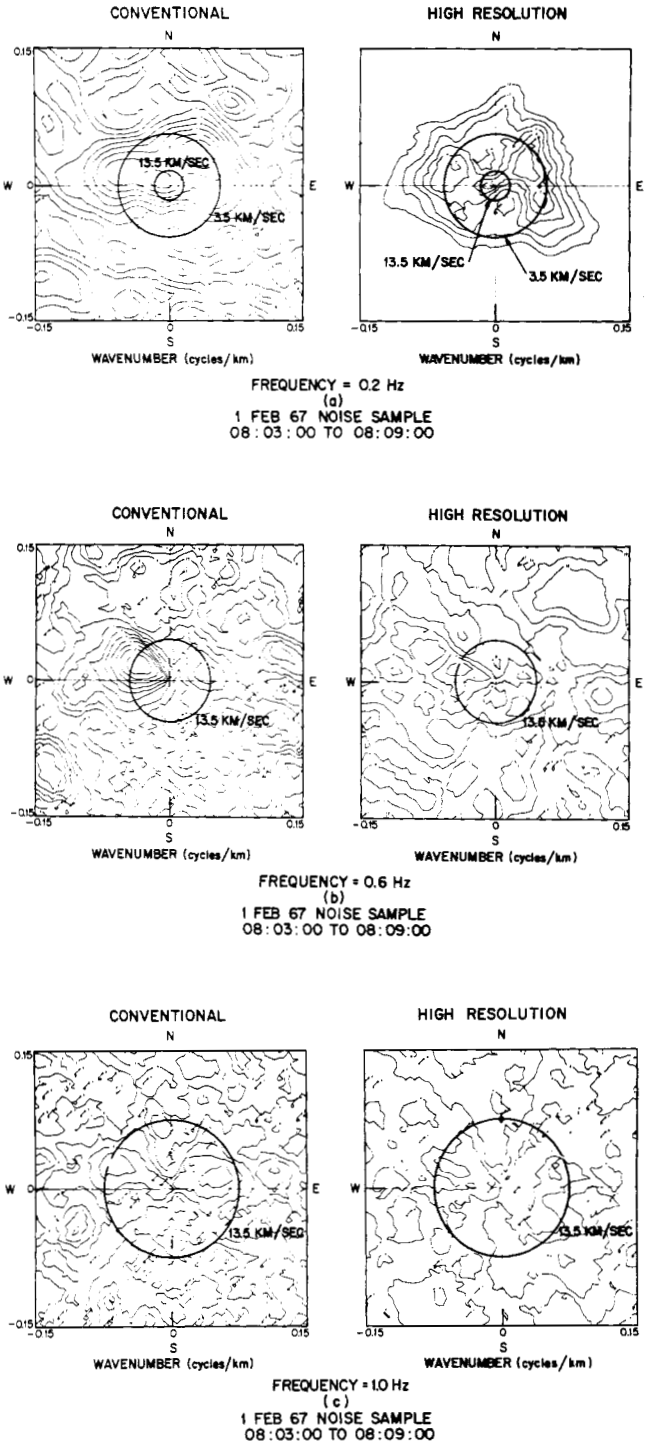


Fig. 10. Conventional and high-resolution frequency-wavenumber spectra for 1 February 1967 short-period noise sample: 08:03:00 to 08:09:00. (a) Frequency = 0.2 Hz. (b) Frequency = 0.6 Hz. (c) Frequency = 1.0 Hz.

The results of both the conventional and high-resolution frequency-wavenumber spectrum measurements for SP noise are shown in Fig. 10 for a noise sample taken on 1 February 1967. The array of SP seismometers used in this measurement is shown in Fig. 11 and the beam pattern for this array is shown in Fig. 12. The results of Fig. 10 show that at 0.2 Hz the SP noise consists of two components, a high-velocity body wave whose horizontal phase velocity is about 13.5 km/s and a low velocity surface wave whose phase velocity is about 3.5 km/s. At frequencies of 0.6 Hz and 1.0 Hz the SP noise consists primarily of body waves.

## Conclusions

The estimation of the frequency-wavenumber power spectral density is of considerable importance in the analysis of propagating waves by an array of sensors. The con-

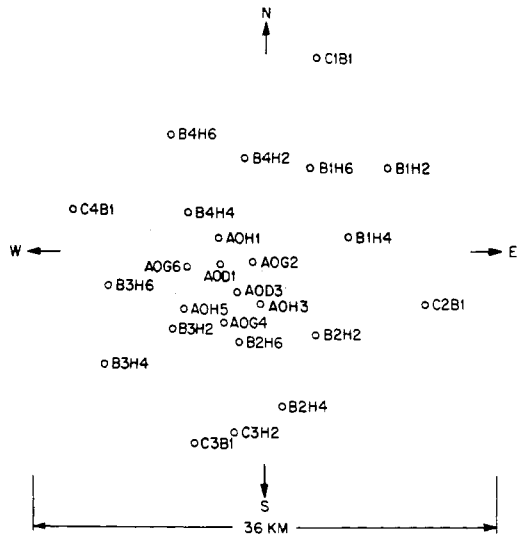


Fig. 11. A subarray of short-period sensors.

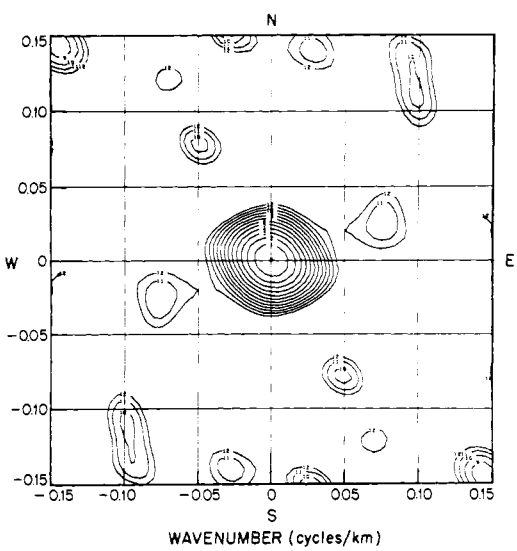


Fig. 12. The beam pattern for the subarray of short-period sensors.

ventional method of estimation employs a fixed wavenumber window, and, as a consequence, the wavenumber resolution is determined essentially by the natural beam pattern of the array of sensors. The high-resolution method of estimation employs a wavenumber window whose shape, and thus sidelobe structure, changes and is a function of the wavenumber at which an estimate is obtained. In addition, this change in wavenumber window shape is performed in an optimum manner, as pointed out previously. As a consequence, it has been shown that the wavenumber resolution of this method is determined primarily by the amount of incoherent noise which is present in the array of sensors, and, to a lesser extent, by the natural beam pattern of the array.

The experimental results show a considerable improvement of wavenumber resolution of the high-resolution method relative to the conventional method. In the case of LPZ seismic noise there was an improvement of about a factor of four, cf. Fig. 3. Thus, the high-resolution method is extremely useful for the estimation of the frequency-wavenumber spectrum when the incoherent noise power is relatively small compared to the power of the propagating waves.

The high-resolution method would, of course, be useful in applications other than seismic arrays. We now mention briefly the application of the method to radio astronomy. It is now possible to synchronize the outputs recorded at several radio astronomy telescopes [9]. Thus, these telescopes can be considered as sensors in an array, (cf. [9, Fig. 1]). If the incoherent noise power in each telescope is sufficiently small, i.e., the radio signals from distant stars recorded by the telescopes should be coherent and there should be relatively little incoherent background noise power, then the high-resolution method is directly applicable for the purpose of using this array of telescopes to map the sources of radio energy.

## References

[1] P. E. Green, Jr., R. A. Frosch and C. F. Romney, "Principles of an experimental large aperture seismic array (LASA)," *Proc. IEEE*, vol. 53, pp. 1821–1833, December 1965.

[2] A. M. Yaglom, *An Introduction to the Theory of Stationary Random Functions*, Englewood Cliffs, N. J.: Prentice Hall, 1962.

[3] J. Capon, R. J. Greenfield, and R. J. Kolker, "Multidimensional maximum-likelihood processing of a large aperture seismic array," *Proc. IEEE*, vol. 55, pp. 192–211, February 1967.

[4] R. B. Blackman and J. W. Tukey, *The Measurement of Power Spectra from the Point of View of Communication Engineering*, New York: Dover Publications, 1959.

[5] M. N. Toksöz and R. T. Lacoss, "Microseisms: mode structure and sources," *Science*, vol. 159, pp. 872–873, February 23, 1968.

[6] W. L. Pilant and L. Knopoff, "Observations of multiple seismic events," *Bull. Seismol. Soc. Am.*, vol. 54, pp. 10–39, February 1964.

[7] J. F. Evernden, "Direction of approach of Rayleigh waves and related problems, Pt. I," *Bull. Seismol. Soc. Am.*, vol. 43, pp. 335–353, 1953.

[8] J. F. Evernden, "Direction of approach of Rayleigh waves and related problems, Pt. II," *Bull. Seismol. Soc. Am.*, vol. 44, pp. 159–184, 1954.

[9] M. H. Cohen, D. L. Jauncey, K. I. Kellermann, and B. G. Clark, "Radio astronomy at one-thousandth second of arc," *Science*, vol. 162, pp. 88–94, October 4, 1968.